Optical microscopy: how nano can you be?

Pavlo Gordiichuk
Zernike Institute for Advanced Materials, University of Groningen, Nijenborgh 4, 9747 AG, Groningen, The Netherlands

Supervisor: Dr. Maxim Pchenitchnikov

Recently a new technique of super-resolution objects imaging based on far-field fluorescence microscopy has been proposed. This technique allows a possibility of super-resolution image development as high as 20 nm in lateral dimensions and 50 nm in the axial direction with fluorescent labels. New imaging technique opens a strong research field in realm of fluorescent labels fabrication and development as a tool of new imaging method. Super-resolution microscopy helps us to reveal the nature of biomolecule self-organization, driving cellular functionalities. There is an essential step of medicine - nano-medicine. The super-resolution methods use different labels for optical imaging without precise understanding of nature of their photo switching. The understanding of nature of these working mechanisms is a challenging task.

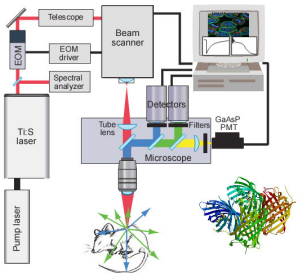

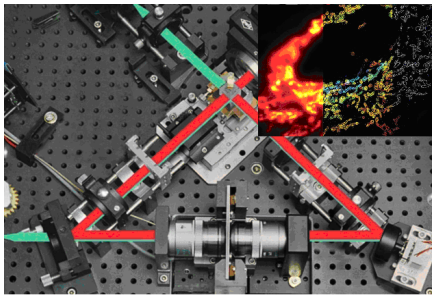

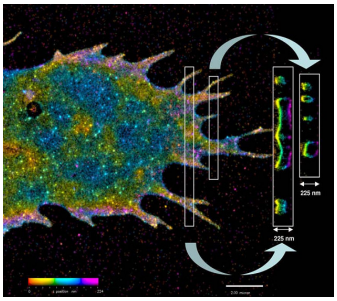

12 August 2010

CONTENTS

I. Introduction

1. Overcoming of optical resolution limit

The understanding of nature of biological process, living cell reactions and moreover its visualization is a desirable aim of biomedical study. The fluorescence microscopy technique enables such possibilities. The specific biological component can be observed via molecular labeling method, and real time observation of living sample can be realized by this method as well. The versatile family of labeling techniques opens a possibility of direct molecular coupling for multicolour imaging of our interest via *in situ* fluorophores hybridization.

Abbe in the 19-th century formulated principle that spatial resolution of optical microscopy is limited by the diffraction of light [1], because $\lambda/2 > 200$nm. The optical resolution limitation leads to development of new methods like near-field scanning microscopy [2], which tries to avoid diffraction limit via approaching scanning tip to the surface. This technique of surface investigation is limited by quality of tip controlling and surface specimen. Another electron microscopy (EM) technique has a high resolution possibility but it is limited by the small number of species, which can be simultaneously observed and also it also uses thin size samples, where we loss volume imaging. In opposite, the far-field light microscopy has essential advantages in comparing to other optical techniques especially for biological imaging. That is why returning to far-field optical technique development is so important.

In recent years new methods were developed which overcome the diffraction limit via application of nonlinear effects to sharpen point-spread function (PSF) of microscope. They are: a stimulated emission depletion (STED) microscope, related methods using other reversible saturable optically linear fluorescence transitions (RESOLFTs), saturated structured-illumination microscopy (SSIM), and techniques that are based on individual fluorescent molecule localization such as a stochastic optical reconstruction microscopy (STORM), photo activated localization microscopy (PALM), and fluorescence photo activation localization microscopy (FPALM) [3]. These methods allow magnitude improvement in three-dimension spatial optical resolution.

To improve optical resolution, the individual labels in resolution limit are isolated one from another by one or more distinguishable optical properties. In this way the position of molecular centers can be determined with a higher precision via statistical fit of ideal PSF to its photon distributions (Figure 1.). In the case when the background noise is small the position of one molecule can be determined with $\sim FWHM/\sqrt{N}$ precision, where N is a number of detected photons, and FWHN is a full width at a half maximum. It is possible to detect 10^4 photons from a single fluorophore with modern technique, which says that single-molecular position in 1 nm precision can be obtained [7]. For increasing single molecular position resolution, the multiple emitters in single diffraction limited region can be isolated one from another by either photobleaching or temporal way (2 to 5 molecules in the region) [4-6]. According to this approach a method for isolation of single molecules at high densities was developed [4]. This method is based on a serial photoactivations and bleaching of scattered photoactivated fluorescent proteins (PA-FP) molecules inside the sample.

The initial image consists of sparse fields of single reversible molecular image positions with weak ground noise when small number of them is activated. The excitation and bleaching of fluorescent molecules are stored for such sparse picture obtaining. Two single images of

molecules will be taken into account for the whole picture if they do not have an overlap (Figure 1.A,C). After applying laser (~λ_{act}) we can activate non-active PA-FPs with the duration and intensity chosen so that the molecular overall density of activated PE-FPs is increased back to a higher value (Figure 1. B, D) [8,9]. This process of activation, measurement and bleaching can be repeated for ~10^5 times for full picture image storages.

The whole *xy* image from different *t* steps overlaps in diffraction limited image (Figure 1.E,F). Gaussian plot fitting allows us to produce more correct position of center point (Figure 1.G). After computer treatment we can obtain the time point-pictures with more robust characteristics (Figure 1. A'-D'). Finally, the picture contains fluorescent molecules in high resolution precise position.

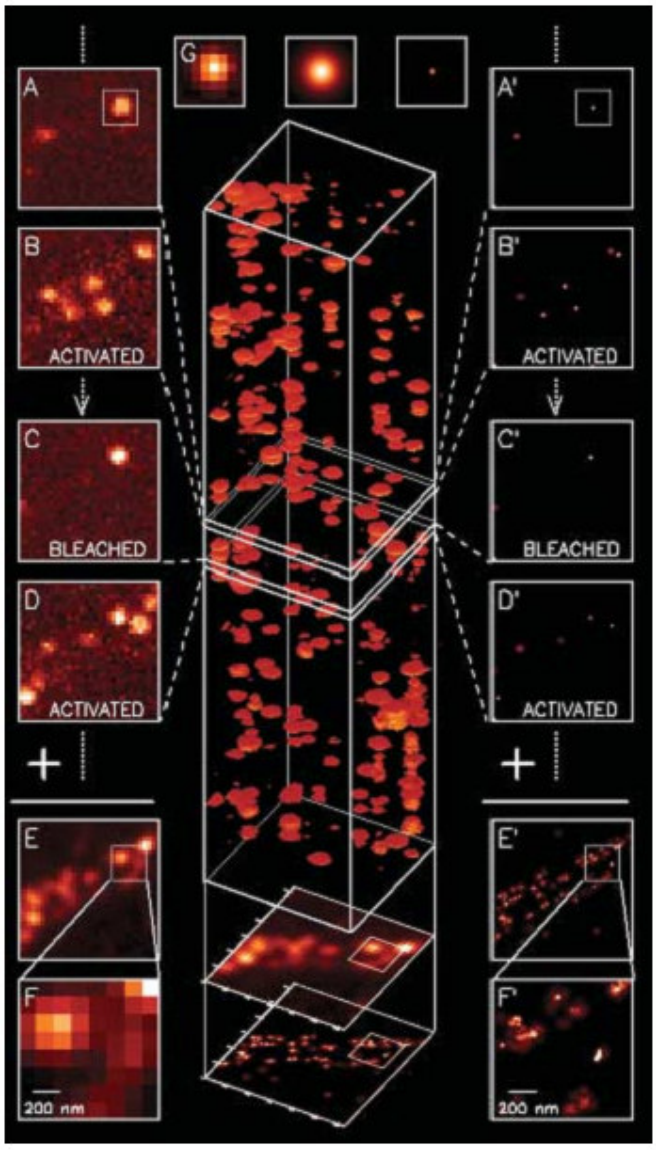

Figure 1. (Aand B) with a brief laser pulse λact=405 mm and then imaged at λexc=561mm until the most are bleached (C). This process is repeated many times(C and D) until the population of inactivated, unbleached molecules is depleted. Summing the molecular images across all frames results in a diffraction-limited image (E and F). However, if the location of each molecule is first determined by fitting the expected molecular image given by the PSF of the microscope [(G), center] to the actual molecular image [(G), left], the molecule can be plotted [(G), right] as a Gaussian that has a standard deviation equal to the uncertainty [4].

2. Single fluorophore label technique

A number of photo-switchable proteins and organic dyes have been applied and their variation of them in the image processes is demonstrated in Table 1. The popular fluorescent proteins have been used for super resolution imaging including KikGR, Dronpa, Dronpa-2, Dronpa-3, FastLime, photo-switchable CFP2 and other photo-switchable organic dyes including

caged rhodamine, caged fluorescein and new developed photochromic rhodamine compound. Increased imaging speeds were demonstrated using asynchronous activation and matching the camera frame rate with the switching kinetics of the fluorophore [12], and also by stroboscopic illumination.

Another important super-resolution possibility is a multicolor imaging; this method requires multiple multicolor optically distinguishable probes. By generalizing their cyanine dye-pair approach, Bates *at al,* have created a palette of photo-switchable probes, each of which consists of a coupled dye pair: this dye can be imaged and deactivated by red light corresponding to its absorption spectrum. For example as many as nine different probes can be formed by combinatorial paring of three reported dyes with different emission wavelengths (Cy5, Cy5.5 and Cy7) and three activator dyes with different absorption spectra (*e.g.,* Alexa, Fluor 405, Cy2 and Cy3). With the help of these probes three-color imaging of DNA on a surface and two-color imaging of immuno-labeled microtubules can be obtained with lateral resolution of ~25nm using two or three different activators each paired with the same reporter [11].

The multicolor super-resolution imaging can be achieved with the help of a photo-switchable organic dye (Cy5) and a photo-switchable fluorescent protein (rsFastLime). According to the fact that these two dyes have different excitation and emission wavelengths, we can use them for two-color imaging for example for microtubes cell imaging. Alone fluorescent proteins are not good for multicolor imaging because they have an overlap of emission spectrum of the pre-activated state and the post-activated state (Table 1). This problem can be solved using a reversibly-switchable green fluorescent protein (Dronpa) and irreversibly switchable green-orange fluorescent protein (EosFP) for two color imaging of actin and adhesion complexes in fixed cells [13]. These two fluorophores are imaged sequentially; Dronpa is imaged after all of the EosFP have been photobleached. For multicolor time resolution imaging we need structures labeled with different colors to be monitored over multiple time points. That is why we need to develop new photo-switchable fluorescent proteins to allow simultaneous multicolor imaging. In addition, Andresen et al., who represented new modification of fluorescent Dronpa (blue-shift variant) for simultaneous application with ordinary Dronpa, made the new modification for this purpose.

Table 1

Spectral properties of photo-switchable organic dyes and fluorescent proteins, including the fluorescence excitation and emission wavelengths of the pre-activation and post-activation states, and the wavelength used for activation of the fluorophore

Fluorophore	Activation wavelength (nm)	Pre-activation		Post-activation		Reference
		Absorption maximum (nm)	Emission maximum (nm)	Absorption maximum (nm)	Emission maximum (nm)	
Fluorescent proteins:						
Kaede	405	508	518	572	582	36
EosFP	405	506	516	571	581	37
KikGR	405	507	517	583	593	39
PA-GFP	405	400	515	504	517	38
PS-CFP2	405	400	468	490	511	43
Dronpa	405	–	–	503	518	40
Dronpa-2, Dronpa-3	405	–	–	486	513	41
rsFastLime	405	–	–	496	518	42
Organic dyes:						
Cy5	350–570[a]	–	–	649	670	50, GE Healthcare
Cy5.5	350–570[a]	–	–	675	694	50, GE Healthcare
Cy7	350–570[a]	–	–	747	776	50, GE Healthcare
Alexa Fluor 647	350–570[a]	–	–	650	665	50, Invitrogen
Photochromic rhodamine B	375	–	–	565	580	45
Caged Q rhodamine	405	–	–	545	575	Invitrogen
Caged fluorescein	405	–	–	497	516	Invitrogen

[a] Dependent upon the activator dye if present.

Table 1. Photo-switchable fluorescent proteins and organic dyes.

II. Organic Cyanine Dye

1. Switching mechanism of single dye

For development of photoswitchable fluorescent probes [14, 15] mechanism of super-resolution fluorescence microscopy was proposed for red carbocyanine dyes. These fluorescent dyes can be photoconverted between a fluorescent state and a dark state for hundreds of cycles and emit several thousand detected photons per switching cycle before diying. The dark state of these fluorescence dyes can be gained by red light and is facilitated with primary thiol in solution. The photoswitchable properties of dyes make them ideal candidates for single molecular imaging. The mechanism of carbocyanine dye photoswitching can be studied from spectrum measurement and mass spectroscopy.

Let's have a look at resolution properties of on/off state switching technique. From ordinary technique of conformation dynamic study of individual bio molecules we know that Förster resonance energy transfer (FRET) is the most widely used. Here the efficiency ε between donor and acceptor fluorophore depends on an intermolecular distance R, with $\varepsilon=1/[1+(R/R_0)]$. The Förster radius R_0 is typically 4-6 nm limited, where the energy transfer is sufficiently bright to be usable for single level detection. Later technique on the base of flavine enzyme was developed, which enables still difficult for 1-3 nm scale resolution. However, recently developed molecules switching based on a cyanine dyes allows decrease spectroscopic rule to probe distance as short as 1 nm. With a help of this technique we have a possibility to down in super resolution microscopy.

This technique is based on cyanine dye (Cy5) as primary chromophore and Cy3 as secondary, which facilitate the switching of Cy5. The single molecule detection can be realized with help of DNA chain to opposite stands. The other part of DNA chain can be immobilized on surface of quartz via a steptavidin-biotinlated BSA linkage.

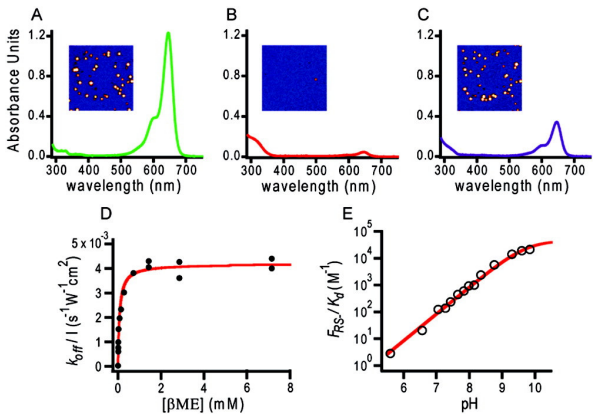

Figure 2. (A) Absorption spectra of Cy5-COOH. The inset shows fluorescence of single Cy5 molecules anchored to a surface. (B) After excitation by a red laser, the Cy5 fluorescence disappears (inset), and the absorption at 650 nm is diminished, while a new peak at 310 nm appears. (C) Following UV illumination, the 650 nm absorption of the Cy5 solution is only partially recovered because of photo bleaching of some Cy5 molecules. (D) The rate constant (k_{off}) for switching off the dye, normalized by the red (633 nm) laser intensity (I), is plotted as a function of [βME] at pH 9.85 (black dots); (E) The fraction of deprotonated thiol normalized by the dissociation constant of the encounter complex (F_{RS}^{-}/K_d) is shown as a semi logarithmic plot against pH.

The work [16] studies a spectrum dyes properties and dark dyes state achievement under thiol molecules influence. The dyes were photoconverted hydrolyzed Cy5-*N*-hydroxysuccinimide ester (Cy5-COOH) in a buffer containing a primary thiol agent, β-mercaptoethanol (βME) (Figure 2. A). The original absorption peak at 650 nm can be reduced by low-intensity red laser light illumination (633 nm or 647 nm) in fluorescent "off" state. As a result the new peak increases at approximately half of the original absorption wavelength (~ 310 nm) (Figure 2. B). The reversible fluorescent active state can be achieved under presence of a nearby chromophore that efficiently adsorbs the activation light, however reactivation of these dyes can be realised also directly without assisting chromophore [16]. The reversible switching of the dark-state into active regime indeed can be realised because of UV absorption peak of Cy5 dark state, which cause such behaviour (Figure 2. C). This reversal procedures allows more than 90% molecules switching efficiency (Fifure 2. insets) [16].

The switching kinetics can be measured via using single-molecule imaging as a function of thiol concentration and solution pH. Both these values have influence upon concentration of deproptonated thiol in solution. At the constant pH value, the rate constant for switching to the dark state (k_{off}) at the first time increases linearly and after saturation at high concentrations of βME (Figure 2.D), which indicates a transition from first-order to zero-order kinetics (Figure 3.).

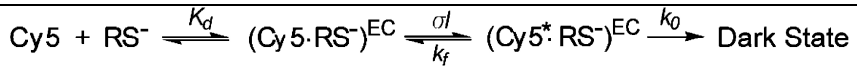

Figure 3. Kinetic Pathway for Dark State Formation. The K_d is the dissociation constant for the encounter complex, σ is the absorption cross-section of Cy5, I is the excitation intensity, k_f is the de-excitation rate constant for the excited dye (Cy5*), and k_0 is the rate constant for formation of the thiol adduct.

The Cy5 makes encounter complex (EC) with thiol anion (RS^-). The light produces non fluorescent thiol–dye adduct, see Figure 3. From (k_{off}/I) data fitting (Figure 2.D) it is possible to obtain normalized fraction of deprotonated thiol (F_{RS}^-/K_d) and quantum yield for dark state formation ($k_0/(k_0 + k_f)$). The data of F_{RS}^-/K_d dependence on different pH values opens possibility to estimate pK_a value (9.74 ± 0.05).

The mass spectroscopy and charge conservation principle from using high-resolution electro-spray ionization liquid chromatography/mass spectrometry (ESI-LC/MS) predicts the way of thiol adding (Figure 4.).

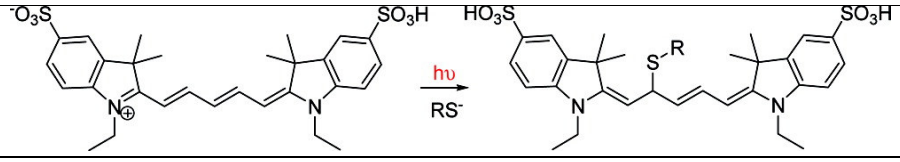

Figure 4. Scheme of thiol adding

We can outline here that the cyanine dyes undergo photo conversion in their dark state under irradiation by red light and it also depends on the supporting of primary thiol in solution. Further experiment with secondary thiol did not produce switching result. That is why such proposed switching mechanism as cyanine–thiol reaction is believed to take place. The switching mechanism represents dependence on primary thiol concentration, where the secondary thiols do

not have such influence. Mass spectroscopy and fragmentation pattern introduces new molecular formation of thiol attachment to the fluorophore Polymethine Bridge.

2. Dye couples as a new labeling tool

In recent years a new family of photo-switchable fluorescent probes was developed and applied to multicolour stochastic optical reconstruction microscopy (STORM) on the base of cyanine dyes. These probes consist of a photo-switchable fluorophore that can be cycled between fluorescent and dark states and activation part for fluorophore activation. Let us discuss the photo-switchable fluorescent dyes [17].

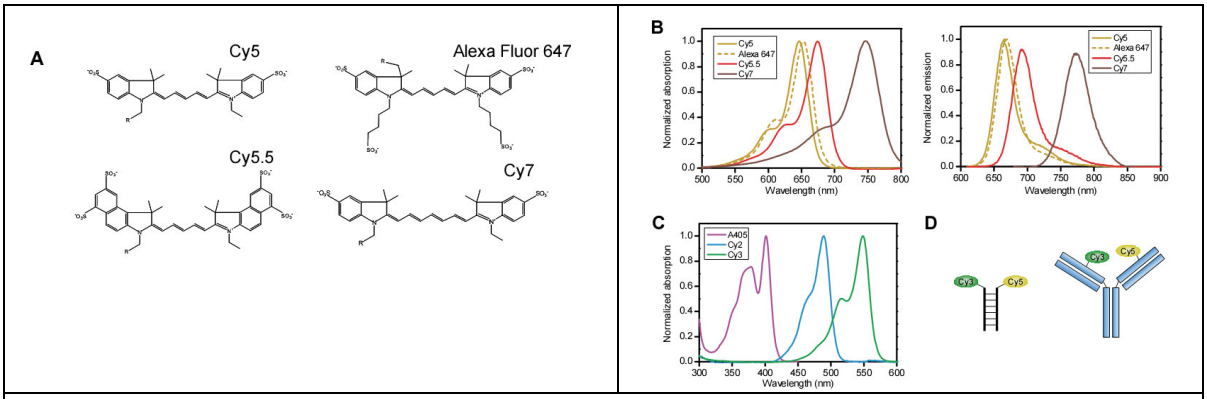

Figure 5. (A) Structures of the photo-switchable reporters Cy5, Alexa 647, Cy5.5, and Cy7. "R" stands for the place where DNA or antibody was attached. (B) Normalized absorption and emission spectra of Cy5, Alexa 647, Cy5.5, and Cy7 in aqueous solution. The absorption spectra were normalized by the maximum absorption value, and the emission spectra were normalized by the integrated peak area. (C) Normalized absorption spectra of activator dyes, Alexa 405, Cy2, and Cy3 in aqueous solution. (D) Schematic of double-stranded DNA and antibody molecules labeled with a Cy3-Cy5 pair [20].

STORM technique allows a possibility of single fluorescent molecular detection with nanometer localization accuracy, because of dye probe application [18, 19]. The photoswitchable probes can be modulated by the fluorescence emission profile of individual fluorophores in any intensity and any moment of activated time. The development of multicolour imaging depends on the construction of bright, photoswitchable probes with different colours. The early work developed a series of dye couples, each of which consists of a cyanine dye molecule with a short-wavelength chromophore [20]. These dye pairs were connected to DNA chain or antibody and immobilized on microscope slides for single-molecule detection (Figure 5.A, D). The robust photo-switching behaviour when paired with a Cy3 molecule in close proximity is represented from a series of cyanine dyes with distinct absorption and emission spectra.

The fluorescent times of multiple switching of Cy5, Cy5.5, and Cy7 with Cy3 as activator are presented in Figure 6. A. The switching between fluorescent and non-fluorescent state are achieved with a help of red laser (657 nm) and green laser pulse (532 nm) respectively, it was mentioned before. The Cy3 dye plays a role of "activator" in switching process, because reactivation of Cy5, Cy5.5, or Cy7 (photo-switchable "reporters") without Cy3 have a slightly optical observation. These switching can be repeated during hundreds of cycles before permanent photo-bleaching. Also it was measured that the number of switching molecules on/off (k_{on} and k_{off}, constant) linearly depends on the laser pulse energy of green and red light, respectively

(Figure 6.B). Moreover, different dyes have different photon emission rates and colours which allow multicolour imaging.

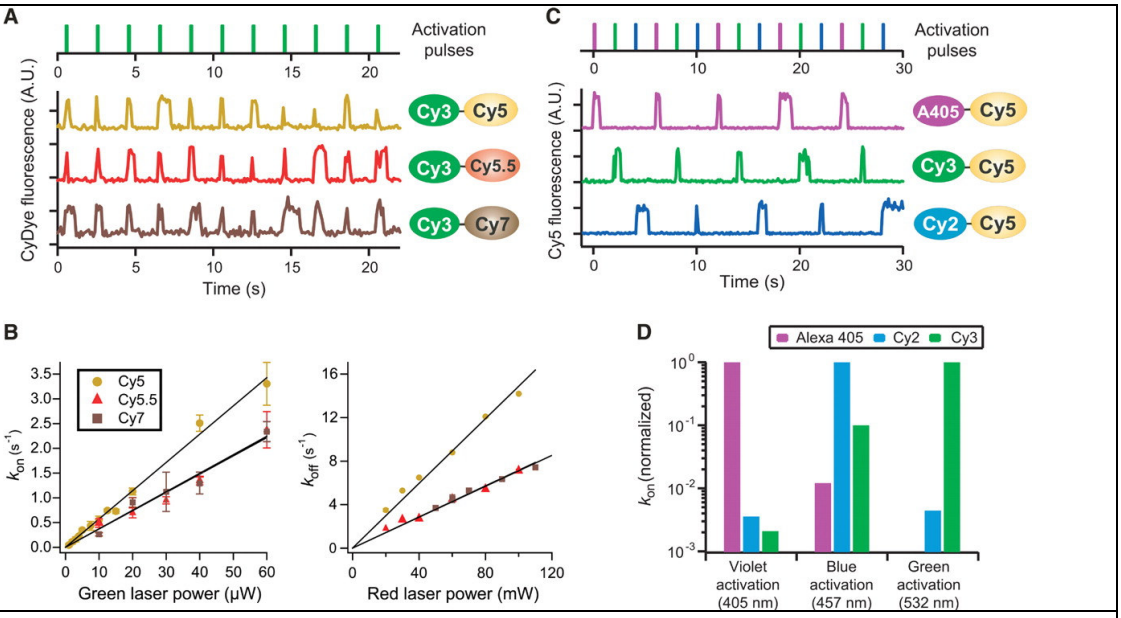

Figure 6. (**A**) Spectrally distinct reporters exhibit photo-switching behaviours. The lower panel shows the fluorescence time traces of three photo-switchable reporters Cy5 (dark yellow line), Cy5.5 (red line), and Cy7 (brown line), each paired with a Cy3 dye as the activator on a DNA construct. (**B**) Switching rate constants k_{on} and k_{off} of the Cy3-Cy5, Cy3-Cy5.5, and Cy3-Cy7 pairs as a function of green and red laser power. (**C**) The same reporter can be activated by spectrally distinct activators. The lower panel shows the fluorescence time traces of Cy5 paired with three different activators, Alexa 405 (magenta line), Cy2 (blue line), and Cy3 (green line). The upper panel shows the violet (405 nm, magenta line), blue (457 nm, blue line), and green (532 nm, green line) activation pulses. (**D**) Normalized activation rate constants of the three dye pairs at three activation wavelengths: 405, 457, and 532 nm. The k_{on} values of Alexa 405-Cy5, Cy2-Cy5, and Cy3-Cy5 were used for normalization at 405, 457, and 532 nm, respectively. The absolute activation rates were rapid for each pair at its corresponding optimal wavelength, with values of 10 s^{-1} or greater at only a few hundred μW of laser power. The activation rate of the Alexa 405-Cy5 pair by the 532-nm laser was too small to be measured reliably.

From further investigation of dye probes construction it was measured that we can use another dye as activation part with different time characteristic (Figure 6.C). The Alexa 405-Cy5 couple was efficiently activated by a violet laser (405 nm) and lees sensitive to blue (457 nm) and green (532 nm) activation light. The same situation was observed for the Cy2-Cy5 pair and Cy3-Cy5 pair which were more sensitive to blue and green lasers, respectively. The activation rate measurement of these dye construction under tree different laser lights shows an excellent characteristic for defined length light switching (Figure 6.D).

3. New fluorescent dye labels modifications

We have already discussed a new technique of dye cyanine labels for super resolution imaging approach in smaller than 1 nm scale and let us see now a possible modification which was developed for cell imaging via application of molecule triplet state. We can make new modifications of single molecule Rhodamine and Pyronin dyes with a help of substitution of

heavy atoms and nitrogen atoms within or close to the external xanthene units of dyes. These modifications were investigated with their present their triplet state dynamics and photostabilities for conditions of ultra-high resolution microscopy. Particularly Rhodamine and Pyronin dyes with a sulfur atom for substitution of the central oxygen atom in the xanthenes unit were found to meet the requirements for ultra-high resolution microscopy, combining a triplet state contribution with reasonable photostability. The switching of dyes into dark, long-lived states, such as triplet state, has attracted interest as a method to achieve ultra-high optical resolution.

The switching of dyes into dark, long-lived states, such as triplet state, is interesting for achieving ultra-high optical resolution. Here we want to transform our disadvantage into our advantages, to use triplet state (which is a disadvantage for reducing quantum yield of fluorophores) as an advantage (as the precursor state from which photobleaching can occur in ultra-sensitive fluorescence microscopy). The new spectroscopic technique which uses its triplet state became possible just a few years ago. It is based on the strategy to minimize the volume of the fluorescence, which is detected by stimulated emission, based on ground state depletion (GSD).

. The ready photo-switchable fluorophores in dark state are required for maximal yield for GSD method and this state can be a triplet molecular state of fluorophores. The triplet state of dyes can be reached with certain additives that enhance photo-induced triplet state generation by removal of dissolved oxygen, and consequently we can observe strong reduction of generation rate of singlet state dye molecules from their triplet state. Nevertheless, this is not always possible for biological cell application.

The physical properties of dyes are limiting factors for all types of fluorescence-based sub-diffraction limit imaging techniques. These limiting factors are based on photo-switching, stochastic photoactivation and single molecule localization. Not all fluorescence proteins can satisfy required conditions and we want to represent some of them in this review. The main aim of these probes application is to develop high quantum yield with stability properties for GSD method application.

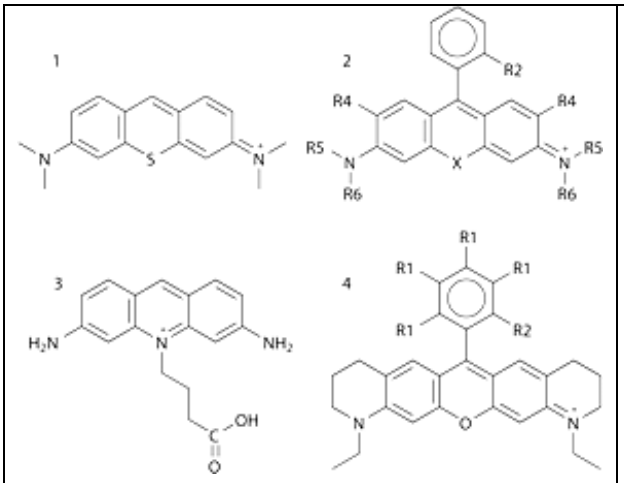

Figure 7. Chemical structures of investigated fluorophores. (1) TP. (2) Rhodamine derivatives, for Rh6G: R2 = $CO_2C_2H_5$, R4 = CH_3, R5 = H, R6 = C_2H_5, X = O; for TMR: R2 = $CO_2C_2H_5$, R4 = H, R5 = CH_3, R6 = CH_3, X = O; for TR: R2 = COOH, R4 = H, R5 = CH_3, R6 = CH_3, X = S; for AT12: R2 = $CON(CH_3)(CH_2)_3COOH$, R4 = H, R5 = CH_3, R6 = CH_3, X = S. (3) ATTO 465 free acid. (4) Halogenated rhodamine derivatives, for DR25: R1 = H, R2 = $CO_2C_2H_5$; for MR71: R1 = F, R2 = $CO_2C_2H_5$; for JA4: R1 = Cl, R2 = CO_2H; for JA98: R1 = Br, R2 = CO_2H.[21]

There are two possible chemical strategy techniques for this kind of dyes preparation. The first uses an atom of sulfur for promoting triplet state build-up due to the heavy-atom effect. At the beginning pyronin dye was used as a frame for chemical development, but resulting molecules of thiopyronin have neither coupling functionality nor desire stability at pH-value

beyond eight. This can be because of inclination to nucleophilic attack with a help of hydroxyl ions of central carbon atom of the chromophore. Finally, development of thiorhodamine is more successful for pH-value stability and reactivity with biomolecules via a NHS-ester coupling group (AT12). The second method of triplet state build-up enhancement is applied on the base of eosin and erythrosine dyes. In these dyes the halogen atom is attached to the xanthene body close to the fluorescently active π – orbital region. Nevertheless, it leads to a high triplet induction much stronger than we need. It is important to investigate a set of rhodamine dye derivatives with halogenated carboxyphenyl group. The molecular structures of TR (thiopyronin), Rhodamine derivatives, TTO 465 free acid and Halogenated rhodamine derivatives, for DR25 dyes are represented in Figure 7. In addition these molecules have more important application for GSD method [21].

III. Fluorescent proteins

1. Green proteins

The super-resolution microscopy image can be obtained also with a help of photo switchable green proteins (GPs), which allow us to go deep in resolution in nm scale. The green fluorescent proteins during last 10 years obtained a wide application in molecular biology, cell biology and medicine. GFP can be used as a biological marker for super resolution imaging. The first observation of bioluminescence (bioluminescence is the process by which visible light is emitted by an organism as a result of the chemical reaction) was made by Pliny [22], which is a reaction of oxidation of the substance by enzyme. There are a lot of biological examples of bioluminescent organisms like in fish, sea cacti, clam, shrimp, and jellyfish. The goal of our work is to study the fundamental background mechanism of photoswitching of these fluorescent labels, which produces this super-resolution possibility.

The *Aequorea* GFP was the first GFP for which the chromophores were cloned and used for different studies. The Shimomura and co-workers isolated a small peptide fragment containing a small chromophore form a papain digest of GFP [23]. He understudied the structure of chromophore by comparing the synthesixing small model compounds with real. The structure of chromophore was represented as 4-(*p*-hydroxybenzylidene)imidazolid-5-one (Figure 8.).

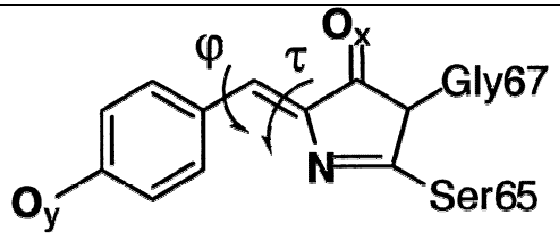

Figure 8. 4-(*p*-Hydroxybenzylidene)-imidazolid-5-one structure of the chromophore. The O_y, O_x, and N atoms shown in bold are possible protonation sites. The φ and τ dihedral angles can rotate in the excited state.

Later it was studied that chromophore which contains peptide fragment is a cyclized hexapeptide formed from residues Phe64-Ser-Tyr-Gly-Val-Gln69 of GFP and a sequence of wild-type GFP. The wild-type of GFP was first determined after understanding cDNA construction, where wild-type contains also Q80R mutation. There are many mutants of GRPs which are very different but their structural features are remarkably similar. The structures of wild-type and S65T were solved for the first time. GFP has specific 11 β-sheet barrel-like

structures with a diameter of about 24 Å and a height of 42 Å. The chromophore is situated in the center of the 11 β-sheets and is connected by α-helical stretch that goes through the center of the barrel-like structure (Figure 9.).

It was studied that the chromophore is formed by an intramolecular cyclization of 65Ser-Tyr-Gly67. This formation is autocatalytic and for this system it needs just external requirement of oxygen presence. The β-can structure protects the chromophore and is responsible for GFP's stability. GFP can be reversibly denatured. There is no fluorescence completely in the denatured GFP. Nevertheless, the fluorescent properties can be gained by β-can structure reconstruction. That is why this technique can be used as an indicator of that the 11-strand β-barrel formation.

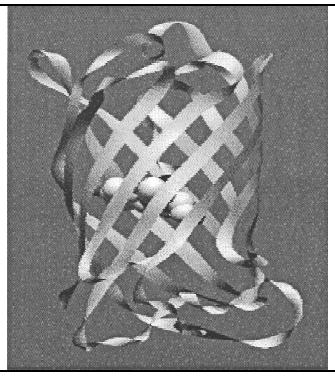

Figure 9. Solid-state structure of GFP. The chromophore is located in the center of the 11-sheet β-barrel and is shown with a CPK representation. (Coordinates for the figure were obtained from the PDB, code 1GFL).

The mechanism of chromophore formation in GFP is a complicated task and can be represented via several stage reactions. Tsien represented the autocatalytic biosynthetic mechanism (Figure 10.) [24]. This scheme follows the spontaneous chromophore formation in a variety of GFP-expressing organisms and they are unlikely to contain the same catalysts during this process. It takes into account the maturation in an anaerobic environment results in a soluble protein (Figure 10. IV), which has the same gel electrophoresis behaviour as GFP but without fluorescence. The procedure of oxygen addition results in step fluorescence (Figure 10. V and VI). The rate of oxidation is different for different GFP mutants.

From adsorption and emission spectrum studies it seems to be little doubtful that a change in protonation is responsible for the different absorptions; however, there is some controversy about the location of the acid- labile site. "From experimental data one can see that the 398 nm absorption is corresponded to a neutral form of the chromophore (HO_Y,N,O_X, Figure 11. A), the absorption at 475 nm to an anionic form (^-O_Y,N,O_X, Figure 11. I), and the red shoulder at 475 nm to a zwitterionic species (^-O_Y,HN^+,O_X, Figure 11. B). The neutral and anionic species are equilibrium ground-states. The concentration of these forms can be changed by changes in ionic strength, protein concentration, pH, temperature and by adding other reagents. From numerical calculation it was obtained that states of proteins are strictly dependent on pH and GFP can undergo five different protonation states over the pH range from −3.2 to 9.4. At pHs over 9.4 it is in the anionic form, between 1.1 and 9.4 it is in an equilibrium between the neutral and the zwitterionic form, and it is in the cationic form (HO_Y, HN^+,O_X) for pHs between −3.2 and 1.1. In the absence of oxygen, mature GFP rapidly turns red, absorbing at 525 nm and emitting at 600 nm. We can say that the photophysical behaviours are unknown" [25].

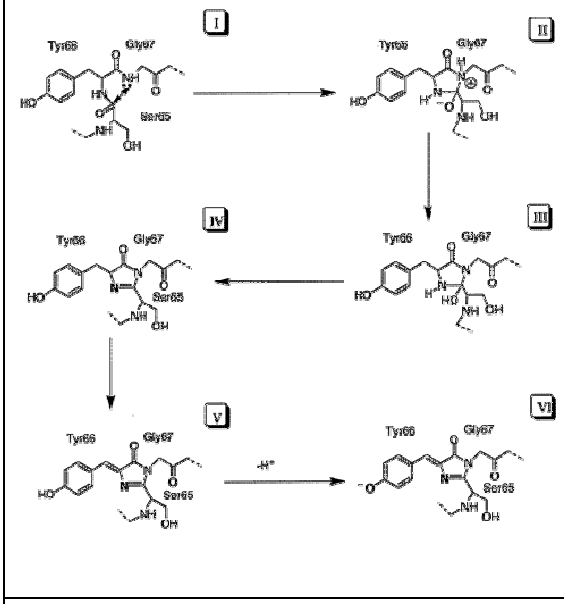

Figure 10. Proposed mechanisms for the chromophore formation in Green Fluorescent Protein [24].

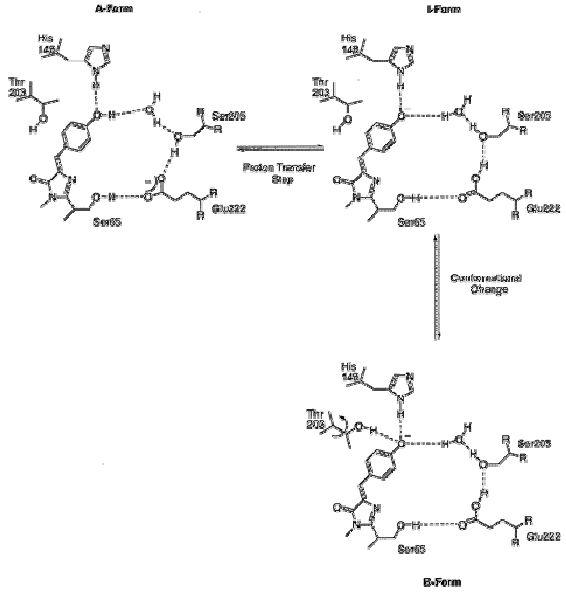

Figure 11. The neutral form (A) can convert to the anionic species (B) via the intermediate state (I). going from the neutral species (A) to the charged species (B), the Tyr66 phenol proton is shuttled through an extensive hydrogen-bonding network to the carboxylate oxygen of Glu222.

The classification of GFPs on the base of spectral characteristics was made by Tsien [26]. "They are the following:

1. Wild-type GFP. The chromophore is in equilibrium between the phenol and phenolate form. It has two excitation peaks at 395 and 475 nm.
2. Phenolate anion (e.g., EGFP). Ser65 has been substituted with Thr, Ala, or Gly. Does not have the 395 nm excitation peak.
3. Neutral phenol (e.g., sapphire). Mutation of Thr203 to Ile results in a mutant that only has the 399 nm excitation. Presumably because the Thr alcoholic proton can no longer have a hydrogen bond to the phenolate, thereby stabilizing it.
4. Phenolate anion with stacked π-electron system (e.g., YFP). Mutation of Thr203 to His, Trp, Phe, or Tyr results in yellow fluorescent proteins.
5. Indole in chromophore (e.g., CYP). Cyan fluorescent proteins have properties intermediate to those of BFP and EGFP.
6. Imidazole in chromophore and phenyl in chromophore (e.g., BFP). Blue fluorescent proteins have an excitation peak at 383 nm.
7. Phenyl in chromophore. This mutant has the shortest excitation wavelength and no apparent usefulness." [26]

2. KikGR, Kaede, EosFP, Dronpa fluorescent labels family

Now we would like to discuss other family of fluorescent probes. Kaede, EosFP, Dronpa, KikG and KikG derivative are widely used for super-resolution microscopy application in the same way. These probes have the same original technique of switching except a new mutant of

KikGRX. The reversible on-and-off switching of green fluorescence (518 nm) can be obtained by using Dronpa. The Kaede protein is a natural fluorescent molecule found in the strongly coral *Trachyphyllia geoffroyi*, with possibilities of irreversible changes in its emission wavelength from green (518 nm) to red (582 nm) upon irradiation of ~400 nm. This protein has a high contrast resolution because of the large shift in emission spectrum and 2000-fold increasing in the red-to-green ration that accompanies the shift. The EosFR is a natural protein found in the the coral *Lobophyllia hemprichii*. The derivative protein KikGR was engineered from KikG protein and a natural green-emitting fluorescent protein found in *Favia favus*, which has also a possibility of green-to-red photoconversion. The common property of these proteins is that they contain triplet His^{62}-Tyr^{63}-Gly^{64}, which allows their conversation between green-and-red states. It is known that this process occurs via a β-elimination reaction that causes cleavage of the His^{62} N_α-C_α bond and the subsequent extension of a π-conjugated system.

The fluorescent protein KikGR was obtained artificially to display a green-to-red photoconvertibility under ultraviolet or violet light irradiation. Like previous similar proteins Kaede and EosFP, KikGR the protein contains a His^{62}-Tyr^{63}-Gly^{64} tripeptide sequence, which forms a green chromophore that can be photoconverted to a red one via formal β-elimination and subsequent extension of a π-conjugated system. Here we want to mention that the double bound His^{62}-C_α and His^{62}-C_β in the red chromophore is in a *cis* configuration, which indicates that rotation along the His^{62} C_α-C_β causes the next cleavage of the His^{62} N_α-C_α bond. The KikGR structural rearrangement causes the evidence that the β-elimination reaction is the main reason of the green-to-red photoconversion.

It is important to note that all photomodulable fluorescent proteins described above thus carry histidine residues near or inside the chromophore. The position of histidine plays different roles in case inside the chromophore (Kaede, EosFP, and KikGR(X)) or outside (photoactivatable GFP and KFP1) it.

A new KikGR protein was later obtained with sodium chloride as a precipitant from natural KikG green-emitting fluorescent protein. It was proved to be harder to crystallization. The aim of KikGR preparation is a high pH sensitivity for examination of the β-elimination reaction kinetics because only excitation of the protonated form of the green chromophore leads to photoconversion. As a result KikGR mutant has high pK_a value in the green state. This protein mutant can be isolated by four residue substitutions, L12M, E70K, P144S, and Q198L, and it keeps the same properties and has been named "KikGRX". The amino acid chains of KikG, KikGR, and KikGRX are shown in Figure 12. A. The photo conversion of KikGRX is shown in Figure 12. B, C. We see crystallographic symmetry generated a tetrameric structure similar to DsRed protein in both cases, Figure 12.D.

"However, the structures within and near the chromophore clearly differed in green and red states. While an unambiguous electron density connecting the His^{62}-C_α and His^{62}-N_α was present in green state (Figure 13.A, green arrows), it was obviously absent in the red state (Figure 13.B, red arrows), indicating that a peptide cleavage had taken place" [27]. Figure 13. represents Structural Basis for the Green-to-Red Conversion. The electron density maps representing the green-emitting chromophore molecular structure (unconverted) state are viewed from the top (top panel) and side (bottom panel) of the chromophore plane (Figure 13. A). "The

connection of His^{62}-C_α and His^{62}-N_α is presented in green (A, green arrows), but not in red (B, red arrow). The structure has *cis* configuration of the C = C double bond in the (5-imidazolyl)ethenyl group of the red-emitting chromophore (Figure 13. B). Figure 13. C, D represents a structure of β-elimination and extension of the π-conjugated system in KikGRX or Kaede and EosFP, respectively. The structures have been derived from Phe^{61}, His^{62}, Tyr^{63}, and Gly^{64}; the position of neighbouring amino acids is also shown (single-letter code). In red state of chromophore C = C double bonds in the (5-imidazolyl)ethenyl group and the neighbouring bonds are red coloured" [27].

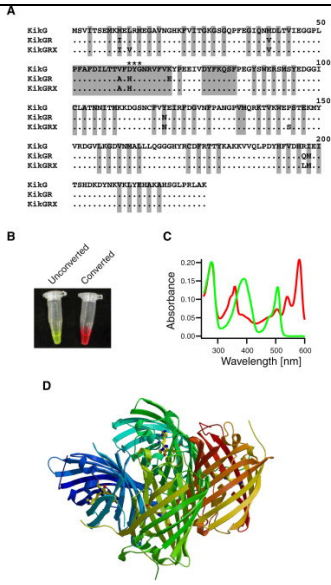

Figure 12. Generation and Characterization of KikGRX

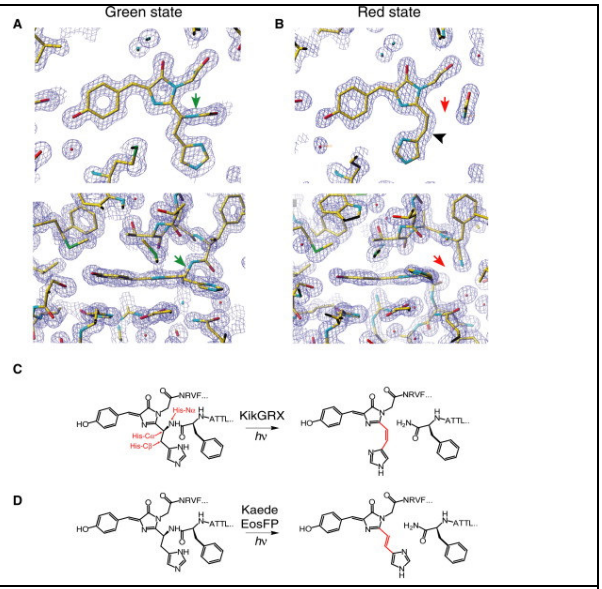

Figure 13. Structural Basis for the Green-to-Red Conversion

The important characteristic of KikGRX mutant is a red-emitting rearrangement. This protein possessed a *cis* C=C double bond in the (5-imidazolyl)ethenyl group (Figure 13.B, and Figure 13.C). From following pictures it is clear that the rotation of imidazole ring along the His^{62} C_α-C_β bond follows peptide cleavage. This is a different situation in comparing with the Kaede and EosFP proteins [28, 29]. It opens a new point of view on reaction mechanism, which was before. The mechanism of this reaction was presented by [27] authors, where they also made some proposals for reconsidering of early mechanisms.

3. E2 or E1 mechanism of KikGRX reaction?

Herein we would like to discuss the possible modified mechanism for KikGR(X) protein switching. From perviously mentioned structural rearrangement we see that the β-elimination reaction leads to the green-to-red photoconversion proceeded by the E1 mechanism. Figure 8 presents a new model of restriction chain for the photoconversion of KikGR(X) versus Kaede and EosFP.

The hydrogen bonding between N_δ of His^{62} and O of Phe stabilizes a green state of His^{62} (Figure 14.A). Because the phenolic hydroxyl group is in its protonated state, the chromophore is excited (Figure 14. B). Further, we see an excited-state proton transfer, which produces ionization of the phenolic hydroxyl group (Figure 14. C). In an ordinary case in *Aequorea* GFP, we see Glu^{222} as an acceptor proton part, but in the case of KikGRX there are no any acceptors. That is why proton transition is possible via hydrogen bonding (Figure 14. C). Photoexcitation produces structural cleavage of the N_α-C_α bond of His^{62} through two mechanisms (Figure 14. D).

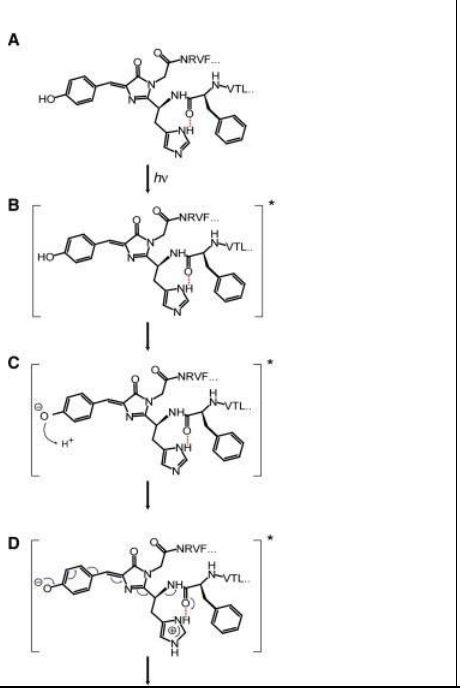

Figure 14. E1 Reaction Model for the Green-to-Red Photoconversion of Fluorescence Proteins

Cleavage generates a hybrid of two structures (Figure 14.E), because the excited ionized phenolic hydroxyl group donates electrons to the π-conjugated system, and the protonated imidazole ring of His^{62} behaviours as an acid, which produces protonating of the carboxamide group (Figura 14.E). From this position E system can be stabilized by carbocation in the E1 elimination reaction. The hydrogen-bonding interaction between N_δ of His^{62} and O of Phe^{61} is destroyed by obtaining free rotation of the imidazole along the axis between His^{62}-C_α and His^{62}-C_β (Figure 14). We see here characteristic properties of KikGRX, the ring flips around in KikGR(X) (Figure 14.H), which does not take place in (Figure 14.F).

We can make some qualitative outlines from this family protein interaction about modern understanding of this mechanism. It is essential to know for fluorescent proteins where a protein does contain a histidine. Histidine plays different roles for (pH sensing properties) depending on whether it is situated outside the chromophore (photoactivatable GFP and KFP1) or within the chromophore (Kaede, EosFP, and KikGR(X)).The hydrogen-bonding interaction between the N_δ of His^{62} and the O of Phe^{61} is important because it stabilizes the imidazolium ring of His^{62} and also allows His^{62} to supply a proton to the carboxamide leaving group. The proposed results [27] (represent) show that there is a flipping of the His^{62} imidazole ring in KikGRX protein which is opposite to EosFP. This flipping produces *cis* formation construction which is opposite to *trans*

conformation in other proteins and this fact has been proved by emission of red state of KikRGX protein. The unstable *cis* orientation of KikGRX protein can be saved by β-can cavity formation. Also we see some doubts in photoswitching technique proposed before. The E1 photoconversion technique is more applicable and answers some questions which were unknown from E2 mechanism, for example, why does the green chromophore must be in its protonated state in order to undergo excitation? Additionally according to photoconversion E2 mechanism the red chromophore of KikGRX is expected to have a *trans* C = C double bond, which is opposite to the results of [27].

4. Dronpa fluorescent molecule

Dronpa is a green fluorescent protein, which was extracted from a coral Pectiniidae. These proteins present perfect properties of switching into the fluorescent "on" state and non-fluorescent "off" state by reversible switching of irradiation of two different wavelengths of light. This mechanism of proteins switching is still open nowadays. There are some predictions in general explanation for the whole molecular construction as donor-acceptor interaction, but not inside atomic construction level. That is why we will try to go on discussing the temporary situation of understanding this mechanism.

To understand the detailed mechanism of the reversible photoswitching process at the atomic level, authors in their recent work [30] performed quantum mechanic (QM) and ONIOM (QM:MM) (Our own N-layered Integrated molecular Orbital and molecular Mechanics. This computational technique models large molecules by defining two or three layers within the structure which are treated at different levels of accuracy) calculations to study the nature of the proposed protein on- and off-states. The authors use several high-level QM methods (TD-B3LYP, CASSCF, CASPT2, and SAC-CI) to compute the vertical absorption and emission energies in the gas phase for four different protonation states as well as two conformations *cis* and *trans* (*cis/trans* construction for anionic, zwitterionic, neutral and cationic protein states). According to the ONIOM (QM:MM) calculation approach the absorption and emission suggest that the neutral *trans* form is the off-state and the anionic *cis* form is the on-state. The authors use Poisson-Boltzman electrostatics and Monte Carlo sampling for calculation of probability of the dominant protonation states.

Photoactivatable fluorescent proteins and particularly reversibly photoswitching fluorescent proteins (RPFPs) have become a new class of fluorescent proteins (FPs). The recent discovery of new RPFP, Dronpa, was made by Miyawaki *et. al.* [31]. Later the authors developed new Dronpa modifications such as Dronpa-2 and Dronpa-3 for a faster response to light and faster thermal relaxation from the off-state to the on-state.

The photoswitching mechanism of Dronpa is a quite complicated mechanism and contains a lot of discussions in its understanding. The obtained emission- absorption experimental results can be explained by Figure 15. The Dronpa produces adsorption peaks in the anion form B 503 nm and neutral form A_1 390 nm of the chromophore. The B form is highly fluorescent (where the quantum yield is equal $\Phi_{fl} = 0.85$, $\lambda_{em} = 518$ nm (2.39 eV), and $\tau_{fl} = 3.6$ ns). From experimental results it is known that the phobleaching, the transition to the nonfluorescent state A_2, was found to occur through intense excitation light of 488 nm, with a

quantum yield (Φ_{PB}) of 0.00032. Moreover, Dronpa can be "activated" to the fluorescent state B by weak irradiation of 405 nm (where the photoactivation quantum yield, Φ_{PA} = 0.37). In addition, the excited state of the A_2 form was found to undergo fast irradiation with less decay (with weak fluorescence of Φ_{fl} = 0.02 and λ_{em} = 450 nm (2.76 eV), which is not presented in Figure 15). Because of existence of non-irradiative metastable form state D was represented from experimental results as a non-fluorescent metastable state. From the first point of view the system works like on single-molecular level. The absorption spectrum of the photoinduced non-fluorescent state A_2 is identical to that of the proposed neutral form A_1 derived from acidification, the latter cannot be photoactivated to the fluorescent state B. The excitation state of proton transfer (ESPT) was represented from the neutral A_2 to give a non-fluorescent intermediate state I (admittedly the deprotonated form in a non-relaxed protein environment) and eventually gives to the anionic B form. This reaction mechanism is similar to the three-state photoisomerization model for wild-type GFP [31].

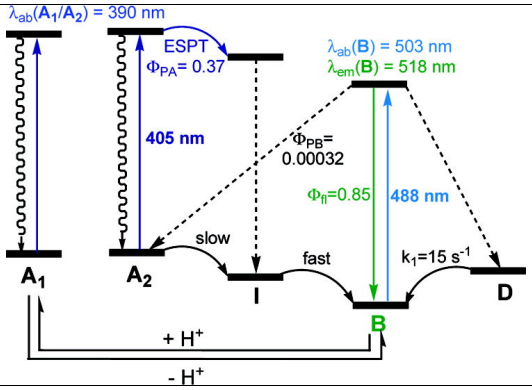

Figure 15. The Proposed Reaction Mechanism for the Reversible Photoswitching in Dronpa

From the pervious protein study it is known that the *cis* and coplanar chromophore conformation corresponds to the on-state crystal structures. In addition, it was suggested that *trans* and no planar conformation causes the off-state crystal structure. [32, 33] From the resent research [30] it has been discussed that the local environment around a chromophore produces an influence to chromophore protonation states. Nevertheless, the conformation mechanism of *cis–trans* isomerization of the chromophore was proposed to lead the protonation state and, in its turn, the on/off-states rather than the reaction mechanism initiated with excited-state proton transfer (ESPT) (Figure 15.) [30].

The detailed reaction mechanism on the atomic level of the reversible photoswitching in Dronpa remains unsolved. The knowledge of characteristic nature processes of experimentally observed on- and off- states will allow us of essential understanding of chromophores photoswitching reaction mechanisms. The finding of this solution for chromophore protonation state is a challenging task, where a lot of protonation schemes have been discussed to be responsible for green fluorescent proteins (GFP). In the recent works scientists present new numerical calculation techniques for investigation of nature of chromophore on- and off states. They try to obtain results via calculation of the vertical adsorption and emission energies of the chromophore with different possible protonation states in the gas phase and in proteins. Moreover, the protonation probability of the chromophore in protein was studied, and scientists tried to develop a possible reaction mechanism, where they can take into account an influence of

environment, which plays an important role for stabilization of *cis* form of the chromophore [30].

The different possible protonation states of the truncated chromophore models are represented in Figure 16, where the gas-phase optimization has been performed by B3LYP/6-31+G(d,p) and two-state-average SA2-CASSCF(14e,13o)/6-31G(d) (S_0:S_1 = 0.5:0.5) methods. The absorption and emission energies of the optimized structures were calculated by TD-B3LYP/6-31++G(d,p), CASPT2(14e,13o)/6-31G(d), and SAC-CI(Level2)/D95(d) methods .

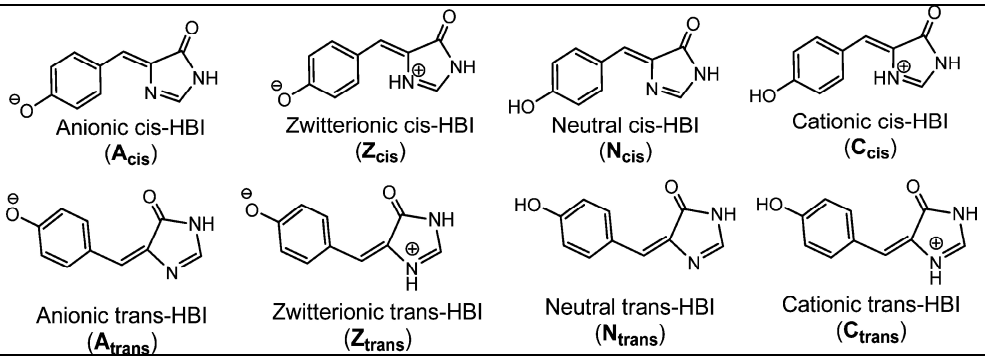

Figure 16. Possible protonation states and conformations.

There are several approaches how to modify numerical calculation when performing ONIOM calculations. One can treat the interaction from the molecular mechanic (MM) point charges with the quantum mechanical (QM) part in the MM (called mechanical embedding or ME scheme) or in the QM Hamiltonian (called electronic embedding or EE scheme). Geometry optimization has been performed in both schemes EE and ME. Gaussian default scaling parameters for the boundaries have been used to avoid over-polarization of the QM wave function. Several QM models are presented in Figure 16. They were obtained in ONIOM calculations to examine the effect of influence of some protein residues in QM calculations.

From the theoretical calculation method we can outline the difference between structural orientation of the chromophores in gas and protein environment. The ONIOM-ME ground structure in protein phase is very similar to the gas-phase structure. The major difference is that while the chromophore for both A_{cis} and N_{trans} is coplanar in the gas phase, the chromophore for N_{trans} in the off-state protein becomes substantially nonplanar with the dihedral angles around two exocyclic bonds φ and τ of the chromophore (in Figure 17) to be 13.9° and −0.4°, respectively. This non-planarity is the result of rotation around the C−C bond (R6), where the chromophore for A_{cis} in the on-state protein is more coplanar (φ = −7.6° and τ = −178.1°).

From the recent X-ray crystal structure research we can outline that the chromophore adopts the *cis* conformation in the on-state Dronpa and the *trans* conformation in the off-state Dronpa [30]. The general ONIOM SAC-CI calculations show that the small and large QM models (MS and ML1) for the chromophore have similar absorption energies for the same protonation states, disregard the on- or off-state protein. The absorption energy for A_{cis} (2.26−2.36 eV) is in good agreement with the experimental value of the on-state Dronpa (2.46 eV). Moreover, the absorption energy for Z_{cis} is also close to the experimental data (the calculation of protonation probability we will discuss later). The absorption energy of the non-planar in the off-state protein (3.01−3.03 eV) is consistent with the experimental one (3.18 eV), but only for non-protonated case.

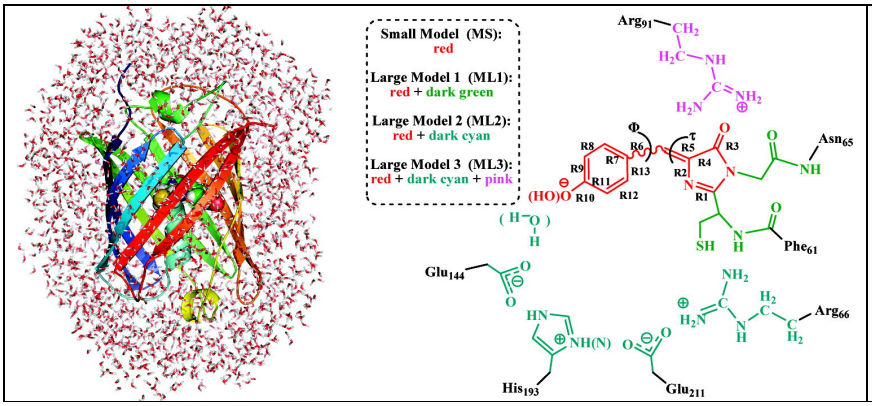

Figure 17. Structure and QM Models in the ONIOM Calculations

Let us discuss a protein effect here. For the investigation of protein effect influence on absorption energy of A_{cis} and N_{trans} we need to take into account the effects of nearby key charged residues in the QM model (ML2 and ML3, see Figure 17). From the ONIOM SAC-CI the calculated absorptions are slightly influenced by this QM effect of the nearby residues (A_{cis}, 2.35 eV for ML2 and 2.45 eV for ML3; N_{trans}, 3.07 eV for ML2 and 3.03 eV for ML3), which are similar to those for MS and ML1. The high quality agreement with experimental data was obtained during increasing of ONIOM measurement precision.

The influence of protein on the absorption and emission spectrum of the chromophore can be separated into two parts: the electronic effect and the geometrical effect. The geometrical effect can be attributed by the protein effect on the chromophore geometry, and can be evaluated as the absorption or emission energy difference of the QM part optimized in the gas phase and that in the ONIOM-optimized protein. The electronic effect includes QM–MM electrostatic interaction, as well as electronic polarization of the QM part due to the MM point charges.

From the theoretical calculations of the absorption and emission energies we can draw conclusions that A_{cis} and N_{trans} are represented as the dominant protonation states of the chromophore in the on- and off-states of Dronpa, respectively [34]. Moreover, the recent calculations estimated that the calculated absorption and emission energies for the off-state are in good agreement with the experiment only when the protein effects are included [30]. These results support the *cis–trans* isomerization of the chromophore along with the change of protonation state.

Reversible mechanism of photochromic properties of Dronpa still remains interesting and unknown. This mechanism of the photochromic fluorescent proteins is supposed to be controlled by several factors: intersystem crossing, protonation states of the chromophore and conformations of the chromophore. The first version has been presented by Miyawaki and co-workers via excited-state proton transfer (ESPT) from the neutral chromophore in the off-state Dronpa and gives the anionic chromophore in the on-state (Figure 18. A) [35].

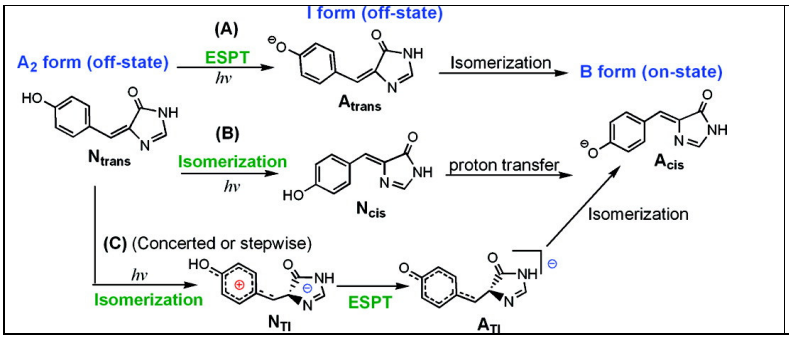

Figure 18. Possible Reaction Mechanisms in Dronpa

The second proposed mechanism involves isomerization of the chromophore, which leads to changes of the protonation state of the chromophore as a feasible pathway; nevertheless the first step of *trans*−*cis* isomerization has open questions (Figure 18. B) [34]. From the recent result from X-ray study we see that the mechanism simply involving excited-state proton transfer (ESPT) without consideration of the *trans* conformation of the chromophore doesn't satisfy existing data of Dronpa off- state. A new technique was presented in Figure 18. C, as it was mentioned before because of conformational change of the chromophore in the off-state crystal structure. In this scheme the excitation of N_{trans} weakens the R5 bond and strengthens the R6 bond (Figure 17.) which cause a facilitate photoisomerization along the R5 bond that gives a stable twisted minimum N_{TI}. Therefore, the acidity of the phenol is enhanced by photoisomerization along the R5 bond, which promotes ESPT to afford an anionic twisted intermediate (A_{TI}) in a concerted or stepwise manner. From the isomerization of A_{TI} eventually we obtain A_{cis}.

IV. Conclusions

Super-resolution technique is a powerful tool for single molecule imaging. As it was mentioned, resolution of 1 nm can be obtained optically with a help of this technique via label protein method and computation results treatment. The resolution of this method also depends on a quality of the measurement equipment, size of labels and its photo switchable optical properties. There are a big number of different fluorescent labels for single molecular imaging, which are widely used without its original mechanism of switching understanding. We tried to discuss these mechanisms of common used fluorescent molecules on basis of new theoretical and experimental results. The optical emission properties of recently discovered dye composition were discussed. The understanding of photo-switching mechanism is important for development of multicolor image application and artificial labels preparing for our direct needs. We also paid attention to attaching possibilities of fluorescent molecules.

Super-resolution microscopy opens possibility for new biological research of living cells. Fluorescent proteins can be genetically fused to any cloned cDNA, proving molecular specificity via functional target proteins. It is a promising technique for original biological mechanism understanding.

Acknowledgments

I would like to thank to my supervisor Dr. Maxim Pchenitchnikov who kindly proposed to me this topic and helped with writing this paper. I also want to thank to Dr. Johan Hofkens and Dr. Antoine van Oijen for discussions and their advice.

Literature

[1] E. Abbe, Beitrage zur Theorie des Mikroskops und der mikroskopischen Wahrnehmung, Arch Mikroskop Anat 9 (**1873**), pp. 413–420.

[2] D.W. Pohl, W. Denk and M. Lanz, Optical stethoscopy: image recording with resolution lambda/20, Appl Phys Lett 44 (**1984**), pp. 651–653.

[3] S.W. Hell and J. Wichmann, Breaking the diffraction resolution limit by stimulated emission: stimulated-emission-depletion fluorescence microscopy, Opt Lett 19 (**1994**), pp. 780–782.

[4] M.J. Rust, M. Bates and X. Zhuang, Subdiffraction-limit imaging by stochastic optical reconstruction microscopy (STORM), Nat Methods 3 (**2006**), pp. 793–795.

[5] E. Betzig, G.H. Patterson, R. Sougrat, O.W. Lindwasser, S. Olenych, J.S. Bonifacino, M.W. Davidson, J. Lippincott-Schwartz and H.F. Hess, Imaging intracellular fluorescent proteins at nanometer resolution, Science 313 (**2006**), pp. 1642–1645.

[6] S.T. Hess, T.P. Girirajan and M.D. Mason, Ultra-high resolution imaging by fluorescence photoactivation localization microscopy, Biophys J 91 (**2006**), pp. 4258–4272.

[7] R.E. Thompson, D.R. Larson and W.W. Webb, Precise nanometer localization analysis for individual fluorescent probes, Biophys J 82 (**2002**), pp. 2775–2783

[8] A. Yildiz, J.N. Forkey, S.A. McKinney, T. Ha, Y.E. Goldman and P.R. Selvin, Myosin V walks hand-over-hand: single fluorophore imaging with 1.5-nm localization, Science 300 (**2003**), pp. 2061–2065.

[9] E. Betzig, G.H. Patterson, R. Sougrat, O.W. Lindwasser, S. Olenych, J.S. Bonifacino, M.W. Davidson, J. Lippincott-Schwartz and H.F. Hess, Imaging intracellular fluorescent proteins at. nanometer resolution, Science 313 (**2006**), pp. 1642–1645.

[10] X. Qu, D. Wu, L. Mets and N.F. Scherer, Nanometer-localized multiple single-molecule fluorescence microscopy, Proc Natl Acad Sci U S A 101 (**2004**), pp. 11298–11303.

[11] S.T. Hess, T.P. Girirajan and M.D. Mason, Ultra-high resolution imaging by fluorescence photoactivation localization microscopy, Biophys J 91 (**2006**), pp. 4258–4272.

[12] M. Bates, B. Huang, G.T. Dempsey and X. Zhuang, Multicolor super-resolution imaging with photo-switchable fluorescent probes, Science 317 (**2007**), pp. 1749–1753.

[13] A. Egner, C. Geisler, C. von Middendorff, H. Bock, D. Wenzel, R. Medda, M. Andresen, A.C. Stiel, S. Jakobs and C. Eggeling et al., Fluorescence nanoscopy in whole cells by asynchronous localization of photoswitching emitters, Biophys J 93 (**2007**), pp. 3285–3290.

[14] Rust, M. J., Bates, M. and Zhuang, X. Nat. Methods (**2006**), 3, 793

[15] Chmyrov, A., Arden-Jacob, J., Zilles, A., Drexhage, K. H. and Widengren, J. Photochem. Photobiol. Sci. (**2008**), 7, 1378

[16] Graham T. Dempsey, Mark Bates, Walter E. Kowtoniuk, David R. Liu, Roger Y. Tsien, *J. Am. Chem. Soc.*,(**2009**), 131 (51), pp 18192–18193

[17] Mark Bates,1 Bo Huang,2,3 Graham T. Dempsey,4 Xiaowei Zhuang, Science 21 September (**2007**): Vol. 317. no. 5845, pp. 1749 – 1753

[18] R. E. Thompson, D. R. Larson, W. W. Webb, Biophys. J. 82, 2775 (**2002**).

[19] K. A. Lidke, B. Rieger, T. M. Jovin, R. Heintzmann, Opt. Exp. 13, 7052 (**2005**).

[20] M. Bates, T. R. Blosser, X. Zhuang, Phys. Rev. Lett. 94, 108101 (**2005**).

[21] Rakesh Kumar Sharma, Shraboni Das and Amarnath Maitra, Journal of Colloid and Interface Science, Volume 277, Issue 2, 15 September (**2004**), Pages 342-346
[22] Marc Zimmer, Chem. Rev., (**2002**), 102 (3), pp 759–782
[23] Shimomura, O. In Green Fluorescent Protein; Chalfie, M., Kain, S., Eds.; Wiley-Liss: New York, (**1998**).
[24] Cubitt, A. B.; Heim, R.; Adams, S. R.; Boyd, A. E.; Gross, L. A.; Tsien, R. Y. TIBS (**1995**), 20, 448−455.
[25] Elowitz, M. B.; Surette, M. G.; Wolf, P.-E.; Stock, J.; Leibler, S. Curr. Biol.(**1997**), 7, 809−812
[26] Tsien, R. Annu. Rev. Biochem.(**1998**), 67, 510−544
[27] Hidekazu Tsutsui1, Hideaki Shimizu2, Hideaki Mizuno, Nobuyuki Nukina, Toshiaki Furuta3 and Atsushi Miyawaki1, Chemistry & Biology, Volume 16, Issue 11, 25 November (**2009**), Pages 1140-114
[28] H. Mizuno, T.K. Mal, K.I. Tong, R. Ando, T. Furuta and A. Miyawaki, Photo-induced peptide cleavage in the green-to-red conversion of a fluorescent protein, Mol. Cell 12 (**2003**), pp. 1051–1058.
[29] K. Nienhaus, G.U. Nienhaus, J. Wiedenmann and H. Nar, Structural basis for photo-induced protein cleavage and green-to-red conversion of fluorescent protein EosFP, Proc. Natl. Acad. Sci. USA 102 (**2005**), pp. 9156–9159.
[30] Xin Li, Lung Wa Chung, Hideaki Mizuno, Atsushi Miyawaki and Keiji Morokuma, J. Phys. Chem. B, (**2010**), 114 (2), pp 1114–1126
[31] Ryoko Ando, Hideaki Mizuno, Atsushi Miyawaki, Science 19 November (**2004**):
Vol. 306. no. 5700, pp. 1370 – 1373
[32] Wilmann, P. G.; Turcic, K.; Battad, J. M.; Wilce, M. C. J.; Devenish, R. J.; Prescott, M.; Rossjohn, J.
[33] Mizuno, H.; Kumar, M. T.; W lchli, M.; Kikuchi, A.; Fukano, T.; Ando, R.; Jeyakanthan, J.; Taka, J.; Shiro, Y.; Ikura, M.; Miyawaki, A. Proc. Natl. Acad. Sci. U.S.A. (**2008**), 105, 9927
[34] Andresen, M.; Stiel, A. C.; Trowitzsch, S.; Weber, G.; Eggeling, C.; Wahl, M. C.; Hell, S. W.; Jakobs, S. Proc. Natl. Acad. Sci. U.S.A. (**2007**), 104, 13005
[35] Fron, E.; Flors, C.; Schweitzer, G.; Habuchi, S.; Ando, R.; De Schryver, F. C.; Miyawaki, A.; Hofkens, J. J. Am. Chem. Soc. (**2007**), 129, 4870